



Natural iron-aluminosilicate as potential solid precursor for supplementary cementitious materials: A comparative study with other aluminosilicates

Joelle Nadia Nouping Fekoua^{a,b,c,f,*}, Paul Venyite^{a,b}, Seunkole Bila^d,
Elie Kamseu^{b,e,**}, Gouet Bebga^f, Myriam Hanuskova^e, Giovanni Dal Poggetto^e,
Sylvie Rossignol^c, Cristina Leonelli^e

^a Laboratory of Applied Inorganic Chemistry, University of Yaounde I, P.O. Box 812, Yaoundé, Cameroon

^b Laboratory of Materials, Local Materials Promotion Authority, MINRESI/MIPROMALO, P.O. Box 2396, Yaoundé, Cameroon

^c UMR CNRS 7315, CEC, Institut de Recherche sur les Céramiques (IRCER), Université de Limoges, 12 Rue Atlantis, Limoges, France

^d Laboratory of Mechanical and Civil Engineering- Polytechnic National High School of Yaounde, University of Yaounde I, P.O.Box 8390, Yaounde, Cameroon

^e Department of Engineering "Enzo Ferrari", University of Modena and Reggio Emilia, ViaP. Vicarelli 10, 41125, Modena, Italy

^f Computational Chemistry Laboratory, High Teacher Training College, University of Yaounde I, P.O. Box 47, Yaounde, Cameroon

ARTICLE INFO

Keywords:

Laterite
Climate-conditions
Supplementary cementitious materials
Géopolymer
Reactivity

ABSTRACT

The objective of this study was to investigate the impact of the geographic and climatic conditions on laterites properties and on geopolymerization based-laterite. Four different laterite deposits in the four geographical zones of Cameroon were studied. This included the center, north, south and west corners of Cameroon, having chemical composition of $\text{SiO}_2 + \text{Al}_2\text{O}_3 + \text{Fe}_2\text{O}_3 = 88.94, 87.6, 89.13$ and 78.97% , respectively. The center and south laterites from the black forest, with high pluviometry and relative humidity, show significant amounts of Fe_2O_3 . While the west laterite from grass field - mountainous areas and the north-laterite from plain arid and semi-arid climate still show lower iron concentrations. The IR absorption bands of the different laterites appear between 1007 and 1047 cm^{-1} ; characteristic bands of aluminosilicate. The BET (Brunauer-Emmett-Teller) Specific surface area values are comprised in the range of $[21.9, 24.1 \text{ m}^2/\text{g}]$ for non-calcined laterite and between $[45.6$ and $123.5 \text{ m}^2/\text{g}]$ for laterites calcined at 550 °C and 575 °C. The main particle size values are $5.71, 6.37, 7.43$ and $8.45 \mu\text{m}$ for center-laterite, west-laterite, north laterite and south-laterite, respectively. Although, they differ in the degree of laterization, all the laterites present almost total conversion to geopolymers, due to the presence of amorphous kaolinite and reactive goethite. However, the iron content has significant impact on the globular microstructure. The particle size of laterites, their high values of BET surface area and their significant reactivity make them promising substitutes to metakaolin and other supplementary cementitious materials.

* Corresponding author. Laboratory of Applied Inorganic Chemistry, University of Yaounde I, P.O. Box 812, Yaoundé, Cameroon.

** Corresponding author. Laboratory of Materials, Local Materials Promotion Authority, MINRESI/MIPROMALO, P.O. Box 2396, Yaoundé, Cameroon.

E-mail addresses: noupiming@yahoo.fr (J.N. Nouping Fekoua), kamseuelie2001@yahoo.fr (E. Kamseu).

<https://doi.org/10.1016/j.heliyon.2023.e17750>

Received 28 February 2023; Received in revised form 22 June 2023; Accepted 27 June 2023

Available online 5 July 2023

2405-8440/© 2023 Published by Elsevier Ltd. This is an open access article under the CC BY-NC-ND license (<http://creativecommons.org/licenses/by-nc-nd/4.0/>).

1. Introduction

In the tropics, iron-rich aluminosilicates, generally called laterites [1] are abundantly available. Many researches have been carried out on their use as aluminosilicate solid precursor [2]. Laterite belongs to the class of clayey materials with kaolinite as principal mineral. Found in tropical and subtropical areas, laterites are formed during the alteration of kaolinitic rocks [3,4]. The process of transformation of kaolinite has been described to take place naturally through corrosion of aluminum minerals, giving birth to iron bearing minerals associated with kaolinite (goethite and hematite) [3]. The particularity of this iron-rich aluminosilicate is its amorphous or poorly crystallized structure. In fact, the kaolinite has some series of octahedral Al^{3+} and Si^{4+} replaced by Fe^{3+} and/or Fe^{2+} . The consequences of these natural chemical inclusions are reduction in crystallinity and increase in specific surface area, with the ability of the particles to flocculate in aqueous solution; indicates that, the reactivity of laterite is achieved between 250 and 800 °C of calcination [5,6] (temperature interval at which the specific surface area increases up to around 120 m²/g). Another research shows that, lateritic bauxites is formed in -situ by the intensive leaching and alteration of the basaltic parent rock, and the process of bauxitization followed the path of deferruginization and destruction of kaolinite [7].

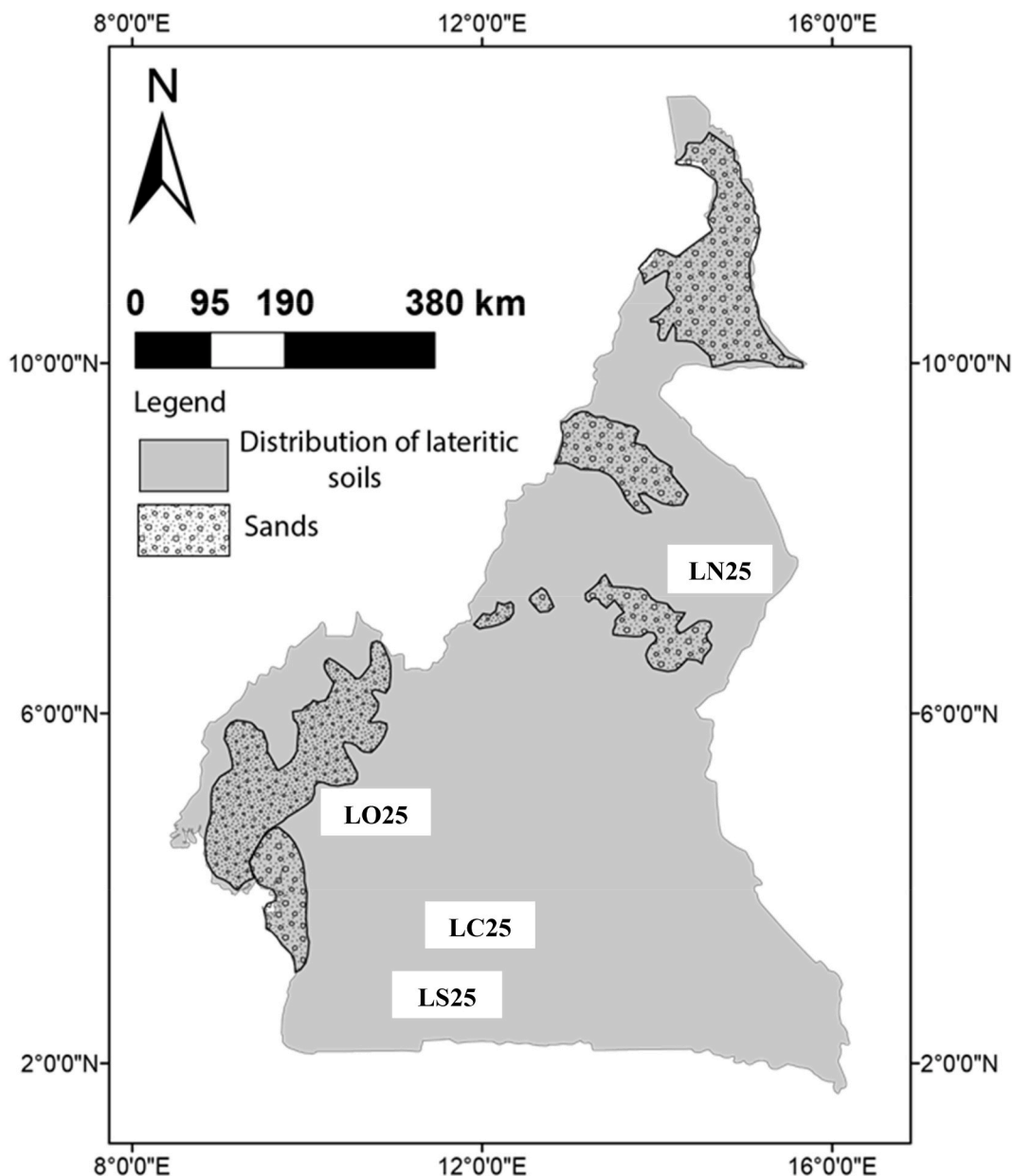


Fig. 1. Distribution of latéritic soils in Cameroon.

The parent materials of tropical soils are weathered under climatic conditions that are favorable for the development of lateritic soils. According to French pedological classification [8], three units of red tropical soils, i.e., ferruginous soils, ferrallitic soils and ferrisols are defined. The results of the analysis of these soils show similarities, as well as differences. Amongst the various soil classifications, ferruginous soils occur in more arid zones with pronounced dry seasons. Ferralsols, and ferrallitic soils occur in more humid areas with dense vegetation. Since each group of soils occurs in regions having different climatic conditions, it is likely that climate plays a major role in development of laterite. [9], in describing the factors that influence soil weathering in tropical regions, placed considerable emphasis on the part played by rainfall distribution, profile drainage, and age or exposure duration to soil forming processes. The following Fig. 1 shows the distribution of lateritic soils in Cameroon. Generally, Cameroon is located in the Central African forest zone between longitude 12.354722 (12°00'E) and latitude 7.369722 (6°00'N), but the areas of interest for this work are central-Yaounde region (Latitude = 03°53'5"N & Longitude = 11°53'0"E), Noth-Ngaoundere region (Latitude = 07°19'0"N & Longitude = 13°34'60"E), South-Ebolowa region (Latitude = 02°54'00"N &

Longitude = 11°09'00"E) and Ouest-Dschang region (Latitude = 5°30'37"N & Longitude = 10°3'12"E). Which Codes are LC25, LN25, LS25 and LW25 respectively.

The use of laterite has been, and is still very common in World [10]. Civil engineering studies of these materials are now in progress, with focus on their use in road and earth dam construction. The main uses of laterites in construction are the production of Compressed Earth Blocks (CEB) [11] and geopolymer [12]. However, they have received very few attentions as supplementary cementitious materials.

Cement is the most important constituent of mortar development. It is well known that the problem of CO₂ emissions into the atmosphere causes a negative effect on the environment and human health. Different human activities including fossil fuel burning, cement production, and deforestation are the main sources of CO₂-emission [13]. That is why many researchers are working on how to substitute the cement content in mortar, without reducing the properties of the final product. On the other hand, aluminosilicate precursors have been identified as corrective additives to mitigate and prevent deteriorative alkali aggregate reactives (AAR) in Portland cement concretes. AAR is a major durability issue of concretes, often referred to as "Concrete cancer". Thus, Metakaolin (MK) and fly ash have been used in many cases as supplementary cementitious materials [14,15]. It has been shown that the substitution of cement by MK in the range of 5–20% can ameliorate concrete properties, including its durability. MK is extensively described in the literature as a solid precursor for the production of geopolymer [16]. As the amorphous Al₂O₃ and SiO₂ contents grow higher than 70%, the capacity to fix chemical ions like Ca²⁺, Na⁺, K⁺, etc, and their high effectiveness in enhancing concrete properties have captured the attention of researchers. Their potential in producing more cohesive and dense concrete also allow their use as supplementary cementitious materials (SCMs) [14,15]. In the case of fly ash (FA), its utilization in mortar/concrete as partial replacement of cement is commonly around 30 wt% and globally, most of the FA is disposed of in landfills which possess environmental problem [17]. For A ground blast-furnace granulated slag their use in the production of construction materials is also to substitute cement in mortar formulation, due to its pozzolanic property. It interacts with calcium hydroxide to form an additional amount of a low-basic hydrated calcium silicate in a hardened cement paste structure [18]. The strength of the blended cement with increasing dosages of slag varies in different ways. Small amounts of slag in cement increase slightly the compressive and flexural strengths in comparison with the blended cement without an additional CEM I. Furthermore, many tests, including thermogravimetric, X-ray fluorescence and X-ray diffractometric analyses have been done on other aluminosilicates (slag, fly ash and pozzolan) and the results show that they can be used for SCMs to reduce CO₂ emissions and mitigate AAR in concrete structures [13,19].

As cementitious materials are the most essential ingredients for concrete, the objective of this study is to investigate the properties of this abundantly available raw material formed in tropical zone (laterite) and exhibit its applicability as industrial supplementary cementitious material. This investigation will stem from the role of climate on the laterization process to the characteristics of the different lateritic materials as SCMs compared to other SCMs.

2. Experimentation and characterization methods

2.1. Raw materials and preparation of alkaline activated laterite

The lateritic soils used in this work were collected in four regions of Cameroon. The first one was collected from Awaé - center region of Cameroon (LC25), the second was collected from Ngaoundere, in the northern part of Cameroon (LN25), the third one was collected from Ebolowa – South of Cameroon (LS25) and the fourth was collected from Dschang – West of Cameroon (LW25). After the collection, all the samples were dried in an oven at 105 °C for 24 h, in order to remove residual water and facilitate the grinding process. In fact, according to previous work, the TGA of laterites show that Physisorbed water is generally evaporated between 45 and 100 °C [20] Then, they were ground up separately to total particles passing through a 75 µm sieve. After which they were calcined at three temperatures (550, 575 and 600 °C) for 4 h at a heating rate of 5 °C/min in a programmable electric furnace. Variation in temperature was done to best activation temperature for each of the soils. The four groups of laterites: non-calcined (LC25, LN25, LS25 and LW25); 550°C-calcined (LC550, LN550, LS550 and LW550); 575°C-calcined (LC575, LN575, LS575 and LW575) and 600°C-calcined (LC600, LN600, LS600 and LW600) were submitted to different analysis. First, to evaluate the effect of the calcination temperature on laterites properties. Secondly, the properties of these calcined laterites were compared to those of MK, FA, pozzolan and slag, with the aim to justify the use of laterites as supplementary cementitious material. Then, 8 M NaOH solution add to each of the non-calcined laterites to study the effect of NaOH attack on the dissolution and reactivity of these raw laterites. Finally, the ability of the raw laterite to develop geopolymerization was evaluated by adding a quantity of rice husk ash (RHA) to different laterites. RHA is a potential source of amorphous silica. The alkaline activated laterite samples were formulated by mixing separately, the non-calcined

laterites with 20 wt% RHA and the 8 M NaOH solution at a constant liquid/solid ratio of 0.6 [21]. The different viscous pastes obtained were poured into cylindrical molds with dimensions 20 (diameter) × 40 (height) cm and sealed in plastic bags in order to prevent water evaporation during the setting and hardening, then, stored at room temperature (25 ± 3 °C) for 24 h before demolding. The cylindrical specimens were labeled GC, GN, GS and GW from the laterites LC25, LN25, LS25 and LW25 respectively, were used to evaluate structural and microstructural properties after 28 days.

2.1.1. Characterization methods

The chemical composition of the lateritic soil samples was determined by X-ray fluorescence (XRF). For this purpose, a good preparation of the material was done. This included the preparation of the pellets by vitrification and the calculation of the loss on ignition. The pellets were made in a furnace at 1600 °C and then X-rayed in the PANATICAL Zetium apparatus at a power of 1 KW.

The particle size distribution was evaluated with HORIBA LA-950 laser granulometer apparatus. The suspension made with water was introduced in the system using Fraunhofer theory. The S_{BET} values were obtained with a Micrometric Tristar II 3020 instrument. The sample was first degassed for 4 h at 110 °C.

To determine the specific surface area, the solids were cooled under vacuum to cryogenic temperature (using liquid nitrogen). Nitrogen gas was dosed to the solid in controlled increments. After each dosage of adsorbent gas, the pressure was allowed to equilibrate and the amount of adsorbed gas was determined. The surface area was then calculated from the amount of gas required to form a monolayer, using the Brunauer Emmett and Teller (BET) equation.

Thermal behaviour was measured using the “SDT Q600 from TA instruments”. The analysis of the materials was carried out under the following conditions: from 30 to 900 °C at a rate of 5 °C/min for 15min. A quantity of approximately 30 mg was introduced into a platinum crucible under a sweep of air. The sample and reference were placed in two identical platinum crucibles.

The chemical bond structures were monitored using Fourier transform infrared spectroscopic measurements, carried out in transmittance mode before being processed in absorbance mode by a “Thermo Fisher Scientific Nicolet 380” spectrometer two operating modes are possible on the instrument: ATR (Attenuated Total Reflection) mode and pellet mode. In the case of ATR, the mixture in the form of liquid to be studied is deposited directly on the diamond and the apparatus is switched on to obtain the acquisitions. The acquisitions are obtained between 500 cm^{-1} and 4000 cm^{-1} . The number of scans is 64 and the resolution is 4 cm^{-1} . In the case of pellets, which have been used in this work, a well ground mixture containing 0.1 g of KBr and a fine quantity of material to be analysed was introduced into a cell and pressed to 10 tons. The resulting pellet was placed in the instrument for characterisation. The OMNIC software was then used for data acquisition and processing in both cases. In order to eliminate the CO_2 contributions from the air present in each spectrum, a straight line between 2400 and 2800 cm^{-1}

The different diffractograms of the powders were obtained on a D8 DAVINCI apparatus using $\text{CuK}\alpha$ radiation such that $\lambda\text{K}\alpha = 1.54186\text{ \AA}$ and a graphite back monochromator. The range of analysis is in the angular range from 5° to 70° with a step size of 0.02 and an acquisition time of 2s. The crystalline phases present in the material were identified using the EVA software.

The microstructure was uncovered with the aid of using a JEOL JSM-6500 F Scanning Electron Microscope (SEM) with an acceleration voltage of 10.0 kV . It is a technical method for surface analysis that permits observations up to nanometric scale. Before being observed, a thin layer of palladium (Au/Pd) was deposited on samples. This metallization avoids the accumulation of charges on the sample surface and reduces the penetration depth of the beam, thus improving the SEM image quality.

3. Results and discussion

3.1. Chemical composition, mineralogy, thermal behavior, particles size distribution and specific surface area of raw laterites

Table 1 highlights the chemical compositions of the four raw laterite samples used in this work. The most dominant oxide in the dark forest laterite of the Centre Region of Cameroon (LC25) is Fe_2O_3 (53%). Even though, SiO_2 (42% and 34%) is most significant in the laterites of the south (LS25) and the west (LW25) zones, Fe_2O_3 is closely followed with 32% and 30%, respectively. The high iron content of the lateritic soils of these zones can be justified by their proximity to the Mbalam and the Nkout iron ore deposits in the South Region of Cameroon. This is equally associated to the high precipitations in these zones, enabling the transportation of leached iron minerals. The hot humid climate could also be a contributing factor, by accelerating the laterization processes. The laterites of the semi-arid zone of the north is significantly dominated by Al_2O_3 , due to the proximity of the three bauxite deposits (Mini-Martap, Ngaoundal and Makan) in the Adamawa Region of Cameroon [22]. The Si/Al molar ratios of 1.1, 0.72, 2.8 and 1.9 for LC25, LN25, LS25 and LW25, respectively, are comparable to good aluminosilicate precursors like MK, fly ash and granulated blast furnace slack, suitable for geopolymerization and SCMs [23,24]. Also, despite the differences in the Si/Al and Si/Fe molar ratios of laterites of the four zones, their $\% \text{SiO}_2 + \% \text{Al}_2\text{O}_3 + \% \text{Fe}_2\text{O}_3 > 90$. This is close with that of highly reactive aluminosilicates like metakaolin and fly

Table 1
Chemical compositions of the raw laterites from XRF.

Samples	Si_2O (%)	Al_2O_3 (%)	Fe_2O_3 (%)	TiO_2 (%)	K_2O (%)	LIO	Si/Al	Si/Fe
LC25	21	16	53	1	1	8	1.1	0.53
LN25	29	34	24	1	–	12	0.72	1.6
LS25	42	16	32	1	1	8	2.8	1.75
LW25	34	15	30	1	–	20	1.9	1.5

ash.

Fig. 2A presents the X-ray diffractograms of LC25, LN25, LS25 and LW25. All the samples have, in varying amounts, the following mineralogical phases: kaolinite, hematite, goethite, quartz and gibbsite. Except for LC25, anatase is equally contained in all the laterites. As shown by the chemical composition (Table 1), the lower of quartz and kaolinite peaks associated with LC25 and LW25 tie with the low SiO₂ content. However, quartz peaks visualized as sand grains are more intense on LW25, which translate that the SiO₂ here is mostly present. In LW25, all the mineral phases are present, suggesting an intermediate stage of laterization. Contrarily, LC25 of the forest zone is composed mostly of goethite and hematite, suggesting an advance stage of corrosion (laterization). The extensive degree of laterization is probably aided by the warm moist environment of the tropical rainforest. Kaolinite peaks are more intense on LN25 and LS25, indicating a more semicrystallized kaolinite phase, different to the quasi amorphous kaolinite phase in LC25 and LW25. The higher levels of kaolinite and gibbsite in LN25 and LS25 are associated to their Al₂O₃ compositions (Table 1). Based on the conspicuous nature of mineral phases in the south forest zone and semiarid northern zone, it is probable that the soils are highly laterized. The advanced corrosive nature of the soils can be associated to the heavy precipitations accompanied by intense sunshine (see Fig. 2).

Fig. 2B evidences the FTIR spectra of different laterites under study. The bands at 3696 cm⁻¹ and 3625 cm⁻¹ are characteristic of the hydroxyl group (OH) of kaolinite goethite and gibbsite [21,25]; confirming their presence in all the four samples. The absorption bands at 3319, 3433, and 3363 cm⁻¹, typical to (d) LW25 correspond to OH stretching of water molecules and organic matter content. This stalemates with the high loss on ignition recorded by LW25 (Table 1). The absorption band at 1027 cm⁻¹ is characteristic of Si–O bonds of crystallized quartz. The absorption band at 1007 cm⁻¹ is the principal band that demonstrates the aluminosilicate: Si–O–M (M = Si, Fe and Al) [26], typical of the laterites under study. The absorption band at 905 cm⁻¹ is linked to Si–O of stretched kaolinite. This band is less intense in LW25, elucidating quite low content of semi-amorphous kaolinite. The bands at 785 and 744 cm⁻¹ are linked to

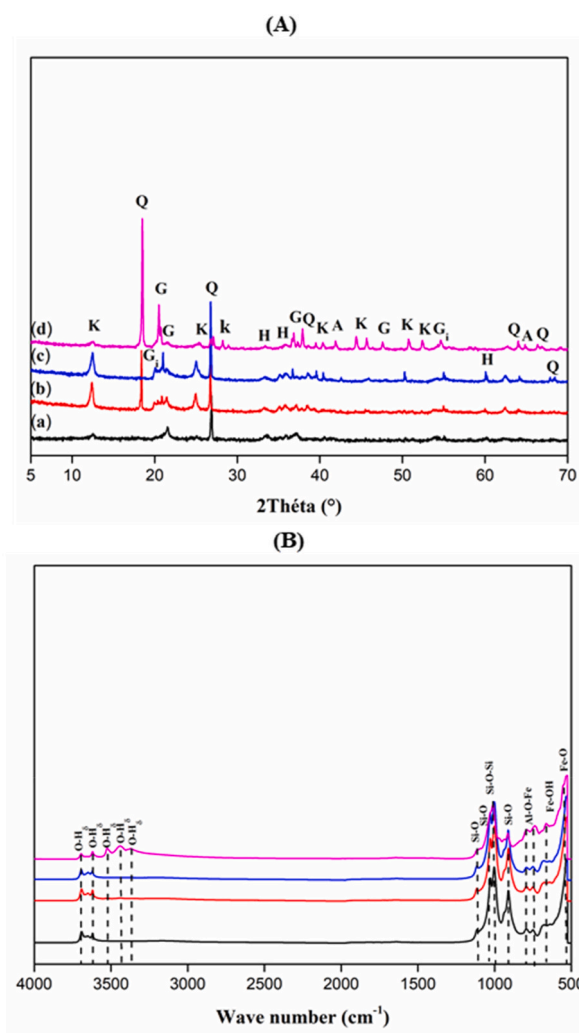


Fig. 2. (A)XRD patterns and (B) FTIR spectra of (a) LC25, (b) LN25, (c) LS25 and (d) LW25 samples. PDF Files: kaolinite (K: 00-005-0143), quartz (Q: 04-006-1757), hematite (H: 04-015-9569), goethite (G: 04-015-8212), anatase (A: 04-014-0490), gypsite (Gi: 00-33-0018).

the Al–OH of gibbsite. The absorption band at 674 cm^{-1} is responsible for Fe–OH bond of goethite. The last band at 532 cm^{-1} is characteristic of Fe–O of hematite.

Fig. 3 highlights the thermal behavior (mass loss and heat flow curves) of the four raw laterites. According to Fig. 3A, each curve presents three thermal phenomena corresponding to the mass loss when physico-chemical reactions happen as laterite are placed in temperature. The mass loss that occurs below $200\text{ }^{\circ}\text{C}$ is due to the loss of physically adsorbed water. This is represented on the heat flow curves (Fig. 3B) of LS25 and LW25 by an endothermic peak. The presence of exothermic peaks on LC25 and LN25 curves can be due to the background during manipulation. Between $250\text{ }^{\circ}\text{C}$ and $350\text{ }^{\circ}\text{C}$, the significant water loss from both samples LN25 and LW25 are 5% and 20%, respectively. The samples LC25 and LS25 seem to have most of their ions in the form of oxides and less hydrated. At around $500\text{ }^{\circ}\text{C}$, the endothermic peaks in Fig. 3B correspond to the decomposition of the mineral kaolinite [27,28]. This decomposition usually takes place at around $575\text{ }^{\circ}\text{C}$ [29]. The relatively low temperature of the decomposition of kaolinite in the laterite is linked to the intensive octahedral substitution of Al^{3+} by $\text{Fe}^{3+}/\text{Fe}^{2+}$, a substitution that significantly reduces the crystallinity of kaolinite and by the way, their anticipates their decomposition. After $500\text{ }^{\circ}\text{C}$ no further mass loss is observed. It can be said that the only difference between these curves and those of kaolin is the mass loss due to goethite decomposition, between 250 and $350\text{ }^{\circ}\text{C}$. Comparing the TGA profile of the four laterite samples, they all have three mass losses. The first corresponds to physisorbed water, the second and the third are associated to OH hydroxyl which is due to the removal of the octahedral Al or Fe ions alongside the concurrent removal of structural hydroxyl groups. This behavior is closely related to those of other aluminosilicates [30]. In fact, according to literature [30], TGA of kaolin shows a weight loss below $200\text{ }^{\circ}\text{C}$ and another one above $450\text{ }^{\circ}\text{C}$, which are represented by two endothermic pics on the corresponding heat flow curves [31]. Concerning Fly Ash (FA), the TGA curve shows three mass loss regions, corresponding respectively to loss of humidity (below $100\text{ }^{\circ}\text{C}$), dehydration ($100\text{--}340\text{ }^{\circ}\text{C}$) and the decomposition of CaCO_3 [32]. According to Ref. [33], slag TGA presents also three mass losses; the one below $200\text{ }^{\circ}\text{C}$ is related to the removal of moisture. To conclude, the thermal behavior of laterite is closely related to that of MK, FA and slag, as the conventional supplementary cementitious material. The main deviations is pointed to the replacement of Al^{3+} with Fe^{3+} and Fe^{2+} ions through the laterization process.

Fig. 4 provides the physical aspects of laterites before and after calcination. Laterites have generally red color due to the high quantities of iron oxide compared to kaolin. The results evidence that when laterites are calcined, the color becomes darker; in

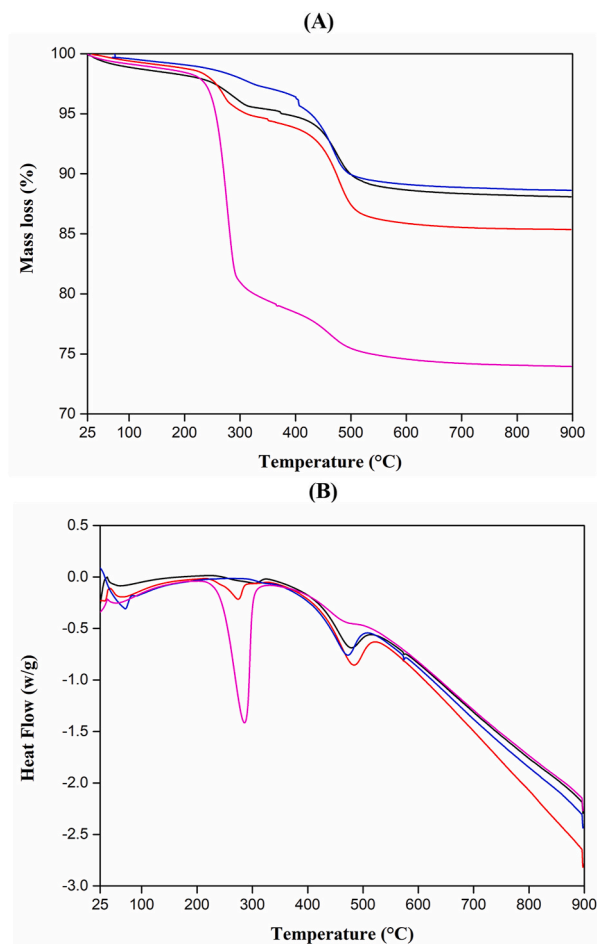


Fig. 3. (A) Thermal behavior and (B) Heat flow of () LC25, () LN25, () LS25 and () LW25 samples.

consequence of the transformation of goethite into hematite, as it has been seen in TGA and DTA curves (Fig. 3A and B). The different colors observed from one sample to another before calcination is due to the quantity of hematite in each sample, based on climatic conditions.

Fig. 5 (5A, 5B and 5C) presents the particle size of laterites samples under this study. From the results, the phenomenon of laterization involves particles coarsening resulting from the iron inclusion and substitution in the kaolinitic framework. The coarse particles of LW25 is obviously affected by the amount of silica with significant fractures. By the way, the volume of fine particles (D_{10}) are around 5.7, 6.4, 7.4 and 8.5 μm for LC25, LW25, LN25 and LS25, respectively. When laterites are calcined at 550 °C, the values are 1.4, 1.6, 2.5 and 1.7 μm , respectively. The result shows that the calcination reduces the finess of powder. When considering D_{50} , MK and laterite have almost similar particles sizes. The laterite from the Northern zone, with high content of alumina (gibbsite) is a little beat coarse. Surely, due to the coarsening of the alumina and silica (quartz). Further sintering seems to impact the coarsening of the alumina particles. Similar observation is made at 575 °C.

However, the cumulative curve of the four laterites is not far from that of metakaolin; (supplementary file). Instead, MK presents more coarse particles ($>50 \mu\text{m}$), compared to laterite. The coarser particles in MK can be associated to the agglomeration of alumina around silica (quartz) grains. This phenomenon is parallel confirmed by comparing the particle sizes of laterites rich in alumina with those pores in alumina. In addition, this phenomenon justifies the absence of particles of more than 364 μm in laterite, compared to MK with particles of more than 470 μm . The calcination of laterites significantly reduces the gap of particles size between MK and laterites.

Table 2 presents the surface area of laterites under study at three different temperatures. At ambient temperature (25 °C), the laterites have SBET values from 20 μm to 25 m^2/g . This is in agreement with those of standard Kaolin (11–25 m^2/g) [34]. When calcined at 550 °C, the values are 46, 29, 34 and 123 m^2/g for LC25, LN25, LS25 and LW25, respectively. The values are 49, 32, 34 and 123 m^2/g at 575 °C. This elucidates that the calcination increase of SBET. Amongst the four laterites, LW presents 123 m^2/g at 550 °C and 575 °C, predicting the presence of the most disordered (amorphous) species in the said sample. It is also the sample with the maximum mass loss after calcination. Fig. 6 evidences the comparative values of chemical composition, PSD and BET of different laterites under study with metakaolin, fly ash, Slag and pozzolan. The values show some similarities and differences, as discussed above, per parameter.

3.1.1. Calcined laterite

The decomposition of the kaolinite mineral and the dihydroxylation of laterite as described by XRD, DTA/TG and SBET (Figs. 2, 3 and 6, respectively) of the raw laterites agree with the evolution of the FTIR spectra of calcined laterites in Fig. 7. In fact, looking at Fig. 7A, B and 7C, when the laterites (LC25, LN25, LS25 and LW25) are calcined at 550, 575 and 600 °C, the absorption bands responsible for O–H water (3519, 3433 and 3363 cm^{-1}) completely disappeared. On the other hand, the absorption bands situated between 905 and 1118 cm^{-1} , corresponding to the Si–O–Si bond are refined to a single and broader band, appearing at 1047 cm^{-1} . This is justified by the increase in the amorphous aluminosilicate content, particularly in silica (Q2 and Q3). Those at 674 and 785 cm^{-1} characteristics of Si–O–Al are distinguished into a unique band at 785 cm^{-1} . Evidence of transformation of crystalline alluminosilicate phases into amorphous alluminosilicate, required for the three dimensional polysialate.

The evidence of the metastability of laterite under study is shown in Fig. 8. Here, all the four laterite samples exhibit significant drops in the intensities of hydroxyl groups (Fig. 8A). This is in accord with the disappearance of kaolinite and goethite peaks on XRD diffractograms in consequence of calcination (Fig. 8B). The absence of Fe–OH, initially present in all the raw materials, at 650 cm^{-1} confirms the transformation of goethite after calcination as, evidenced in Fig. 8A. The shift of the principal aluminosilicate bands to



Fig. 4. Physical aspect of four laterite before and after calcination.

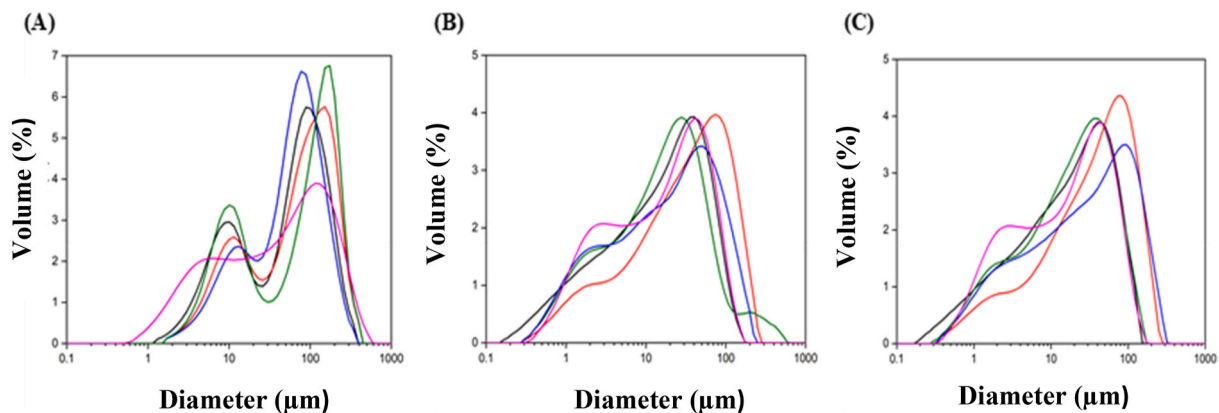


Fig. 5. Volume particles sizes' curves at (A) 25, (B) 550 and (C) 575 °C of () LC25, () LN25, () LS25, () LW25 samples and () MK.

Table 2
Specific surface area values of samples before and after calcination.

Materials	S _{Bet} (m ² /g)		
	T = 25 °C	T = 550 °C	575 °C
LC25	25	46	49
LN25	23	29	32
LS25	27	34	34
LW25	20	123	123

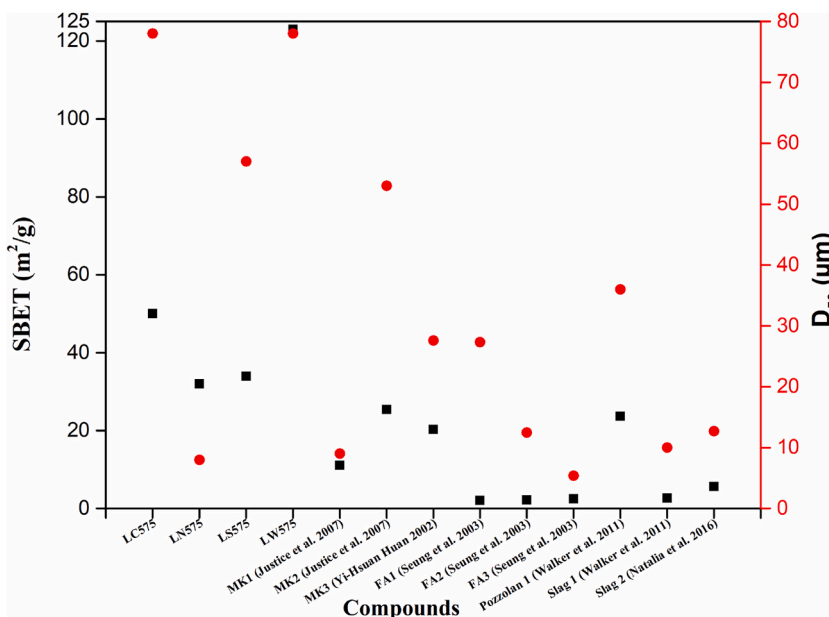


Fig. 6. (■) SBET and (●) D₅₀ of LC575, LN575, LS575, LW575, some metakolin, pozzolan, fly ash and slag collected in literature.

lower wave number (1000 cm⁻¹) also backs the formation of amorphous phase, upon calcination.

3.1.2. Alkaline activated laterites

Fig. 9 presents the FTIR spectra of the raw laterites after attack with sodium hydroxide solution. The bands at 3696, 3319, 3433, and 3363 cm⁻¹, initially observed on the raw laterites' spectra are present on those of the calcined laterites, but, with reduced intensities. The new bands at 1395 and 1468 cm⁻¹ are respectively attributed to water and carbonates (C-O) from Na⁺ ion (of alkaline solution) interaction with the atmospheric CO₂. These bands are more represented in samples synthesized with LC25, LS25 and LW25.

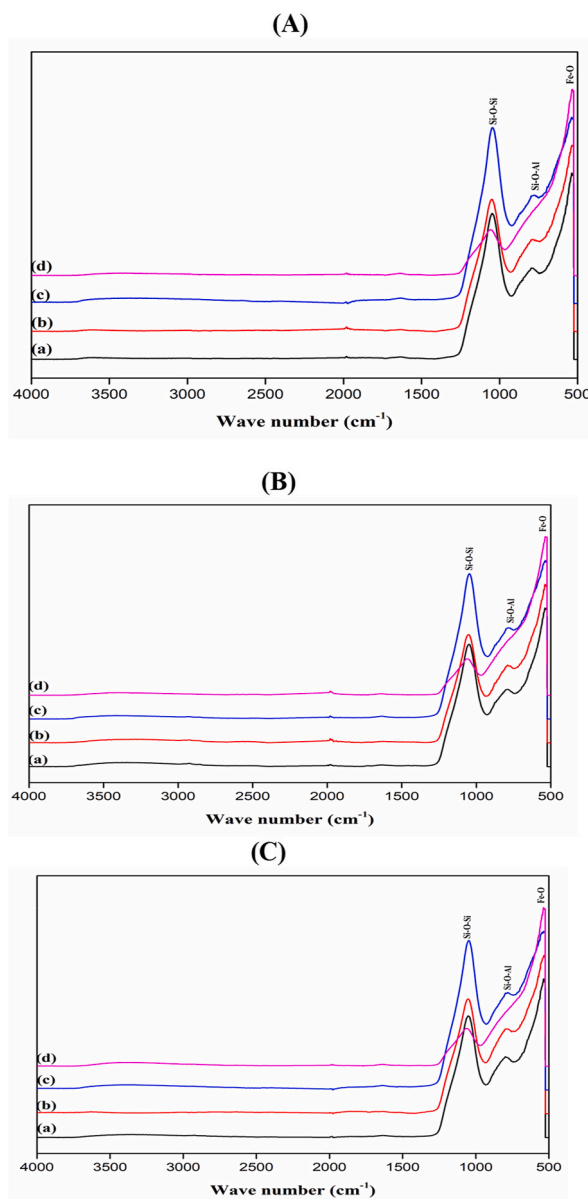


Fig. 7. FTIR spectra (A) 550, (B) 575 and (C) 600 °C of (a) LC, (b) LN, (c) LS and (d) LW samples.

The shift of Si–O–Si band from 1027 to 950 cm⁻¹ can be justified by the formation of three dimensional polysialate network by the polycondensation of the free aluminosilicate units in the alkaline medium [35]. Therefore, in a strong alkaline medium, raw laterites of the four studied zones polycondense to form a three dimensional network consolidate.

Fig. 10 presents the XRD pattern of the study laterites after alkaline activation of raw laterite. The result shows that the raw laterites contain quasi amorphous (stretched) phases with loose bonds that can easily be dissociated in an alkaline solution to form aluminosilicate/ferrosilicate gels. The strong alkaline medium facilitates the dissociation of hydroxyl group linksto the most corroded minerals (kaolinite, goethite and other iron-bearing hydroxides and oxyhydroxides). The most important peaks present on the alkaline activated laterite diffractograms are those of quartz, inherited from the raw laterite. The quartz peak at $2\theta = 20^\circ$ on the northern zone laterite (LN25) diffractogram disappears after alkaline activation (GN), while that of in the west Cameroon (LW25) decreased in intensity. On GS and GN diffractograms, the residual intensities of kaolinite are observed. Reduced hematite intensity is also observed, as a result of the partial dissociation of goethite. Goethite can be dissolved completely in high alkaline solution. In the presence of free silica or aluminosilica, in such alkaline medium, there is formation of ferrosialate, ferrosilicate and/or ferrisilicate, by association with the released iron. The kaolinite present in the laterites has high degree of substitution [36] and insertion of Fe²⁺/Fe³⁺, resulting in a meta stable to amorphous structure, prompt to easily dissociate in strong alkaline solution. The products of the dissolution will polycondense/polymerize to polysialate (-Al-O-Si-O-Al-O) and polyferrosialate (-Fe-O-Si-O-Al-O).

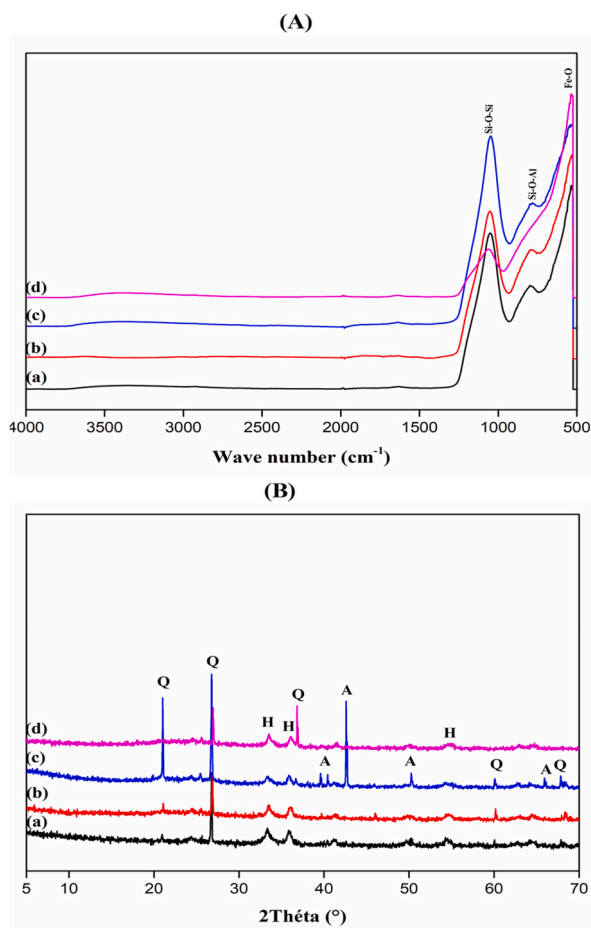


Fig. 8. (A) FTIR spectra and (B) XRD patterns of (a) LC600, (b) LN600, (c) LS600 and LW600 samples. PDF Files: quartz (Q: 04-006-1757), hematite (H: 04-015-9569), anatase (A: 04-014-0490).

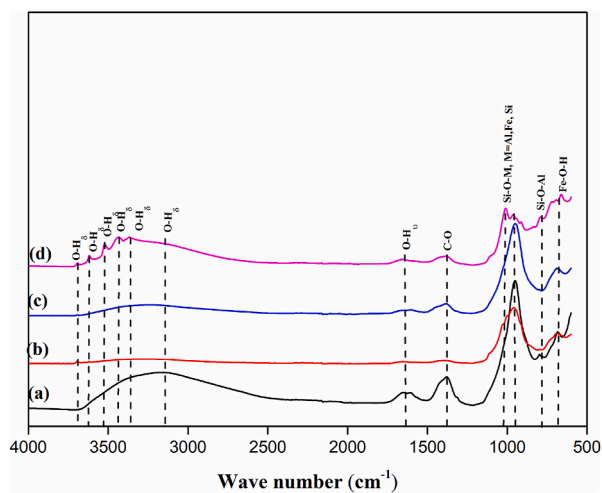


Fig. 9. FTIR spectra (a) LC25, (b) LN25 and (c) LS25 and (d) LW25 after alkaline attack in 8 M sodium hydroxide solution.

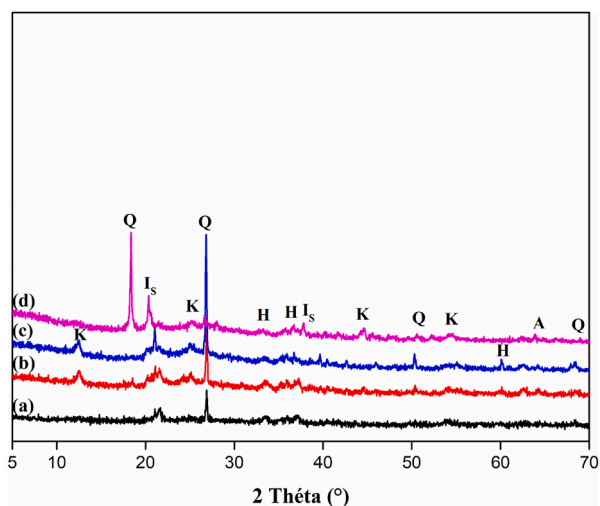


Fig. 10. XRD patterns of (a) GC, (b) GN, (c) GS and (d) GW geopolymer based non-calcined laterites samples. PDF Files: kaolinite (K: 00-005-0143), quartz (Q: 04-006-1757), hematite (H: 04-015-9569), goethite (G: 04-015-8212), anatase (A: 04-014-0490), gibbsite (Gi: 00-33-0018).

The complete transformation of kaolinite minerals in the case of LC25 and LW25 is justified by the climatic conditions (humidity and temperature) that favor the process of laterization in contrast to LS25 that has the required humidity, but not temperature and LN25 that has the required temperature but not humidity.

Fig. 11 presents the micrographs of the different laterites after alkaline stabilization. The micrographs display continuous compact mass; with no visible porosity. GN, GS and GW show the most densified matrices with finer particles, compared to GC that shows some microcracks (Fig. 11A). In fact LC25 presents the lowest silica content (20.51w %) and the highest concentration of iron (52.2%) as it has been seen previously. These effectively modify the Si/Al and Si/Fe ratios with consequence modification of the final volume of gel forming. While all the matrixes still present good densification and compactness, there appear a slight difference on the globular character of the r gels formed. In fact, the $\text{SiO}_2/\text{Al}_2\text{O}_3$ is ≈ 1 for LC25 and LN25, and ≈ 2 for LS25 and LW25. This difference explains why the macrostructure of gel of GS and GW are very closed to that of metakaolin-based geopolymer. In GC and GN more ferrosialate is formed, explaining the slight difference between the matrixes. The reactive silica from the corroded phases provides sufficient colloids to the cement matrix and avoids porosity. This is evidenced in Fig. 11B. While the major part of the reactive silica present in GN, GS and GW seems to be orientated to the formation of N-A-S-H and N-Fe-A-S-H, more colloidal silica is observed in the GC micrograph. It can be noted that, the additional reactive silica conducts mostly to the formation of ferrisilicate. Otherwise, a careful mix design is needed including reactive silica addition. Although there is a difference in the laterization observed, all the laterites present almost total conversion to cementitious polymer phases, due to the presence of amorphous kaolinite and reactive goethite and the globular types of gels are similar to that of MK-based alkaline activated matrixes. The gel formed is likely to be a mixture of N-A-S-H and N-Fe-A-S-H (GN, GS and GW). In addition, the content of iron has significant impact on the globular microstructure.

4. General discussion

In the northern temperate zones of Cameroon, the most used binder and cementitious materials are metakaolin and clinker, which are raw materials that are widely available in this area. In the tropical zone where most countries are in the process of developing research and do not have enough of these materials, researchers are obliged to look at the available resources to develop substitutes to conventional materials. Thus, laterite, a very abundant raw material, available in the tropical zone, has been explored for many years. It should also be noted that in construction, mortar is generally made from cement, which constitutes the main cementitious component. However, cement poses two fundamental problems for the tropical zone: the unavailability of clinker, which implies a high-cost price of the final material and the pollution of the environment by the release of a large quantity of CO_2 into the atmosphere during clinkerization. Faced with these problems, this work aimed to characterize the laterites from different regions of Cameroon, to compare their properties with those of metakaolin, fly ash, slag and pozzolan, which are generally used as supplementary cementitious materials. The results obtained according to chemical composition and FTIR show that the four laterites have oxides $\text{SiO}_2 + \text{Al}_2\text{O}_3 + \text{Fe}_2\text{O}_3 \geq 70\%$ and absorption bands between 1007 and 1027 cm^{-1} . This is in accord with ASTM standard (C618, C125, C989 and C1240), which indicates that a supplementary cementitious material is defined as an inorganic material that contributes to the properties of the cementitious mixture with true hydraulic or/and pozzolanic activities. These properties generally come from.

- (i) Chemical composition: $\text{SiO}_2 + \text{Al}_2\text{O}_3 + \text{Fe}_2\text{O}_3 \geq 70\%$;
- (ii) The disorder structure (XRD semi crystalline or quasi amorphous phases);
- (iii) The particles size distribution (PSD); high content of particles below $10 \mu\text{m}$;
- (iv) High BET values of specific surface area.

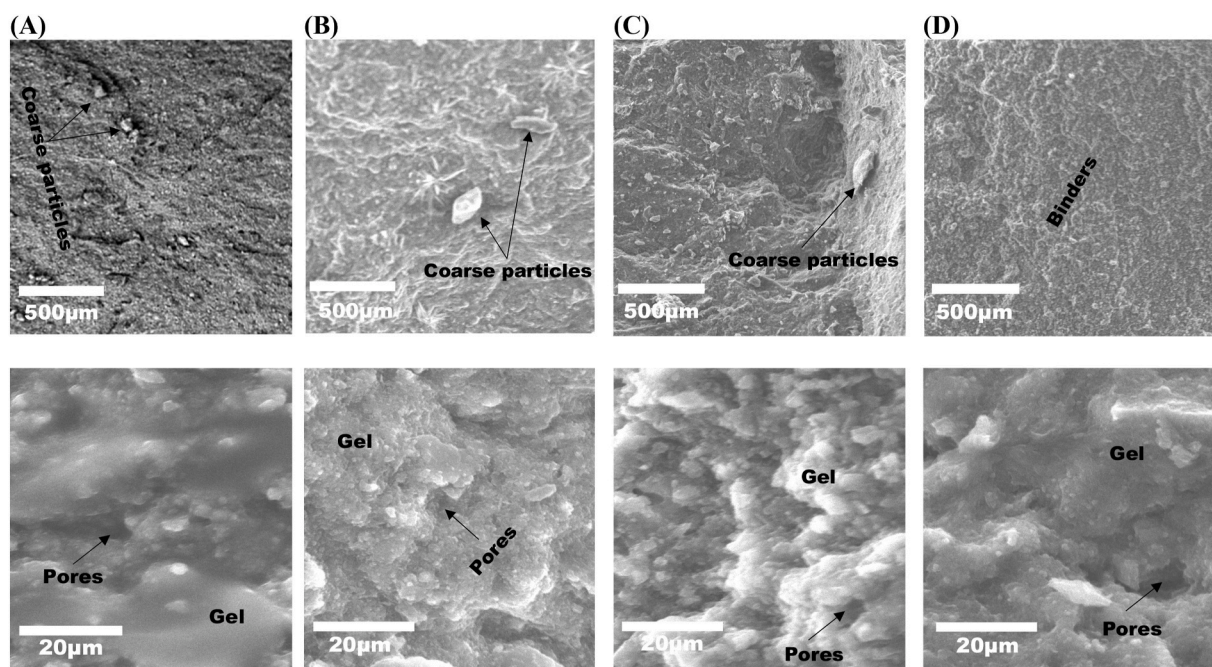


Fig. 11. Microstructure of (A) GC, (B) GN, (C) GS and (D) GW geopolymer based non-calcined laterites samples at different magnifications.

However, the climate plays an important role in the formation of disordered phases, through the laterization process. In rainy areas, the leaching is accentuated and this has an impact on the silica content, which decreases, thus requiring an external contribution of amorphous silica to further activate the laterite. This is the case of LC and LS. In addition, when considering LC and LS from the rain forest, having high pluviometry and relative humidity, they show significant amount of Fe_2O_3 . While LW from mountainous area and LN from the plateau with semi-arid climate show lower iron concentrations. Concerning the mineralogical analysis, the results revealed the presence of pseudo amorphous phases in all the raw laterites (kaolinite, goethite), which play an important role in the reactivity of laterites and justifies the fact that they can play the same role as MK. By agreeing on the BET values, the specific surface values of non-calcined laterites are close to those of metakaolin (Close to $25 \text{ m}^2/\text{g}$) so in terms of reactivity, raw laterites are similar to those of some metakaolin; when laterites are calcined the specific surface area increases, which further improves the properties. In conclusion, it appears from these observations that laterites have properties close to those of metakaolin, and could therefore be used for cement substitution, as supplementary cementitious material.

5. Conclusion

At the end of this work, of which the aim was to evaluate the properties of laterites, to see if they can be used as supplementary cementitious materials, four laterites' types were studied: LC25, LN25, LS25 and LW25. LC25 and LS25 from the tropical rain forest; LN25 from semi-arid plateau and LW25 from mountainous region. Chemical composition, mineralogy, particles size and BET were investigated. The alkaline activation of the raw laterite was also investigated. From the results, the following conclusions can be done.

- 1) Study laterite, are essentially composed of pseudo amorphous kaolinite and goethite, with some of $\text{SiO}_2 + \text{Al}_2\text{O}_3 + \text{Fe}_2\text{O}_3 \geq 70\%$, as in agreement with ASTM standard CM618-19.
- 2) In the natural form, laterites are aggregations of particles that can flocculate at room temperature, justifying the 39.5, 35, 34.5 and 39.4% of passing and 77.85, 57.75, 79.74 and 69.52% for raw and 550°C calcined, respectively. Laterite fulfills the requirements of the ASTM C618-19 for cementitious materials.
- 3) The BET values of the different laterites are between $21.9\text{--}24.1 \text{ m}^2/\text{g}$ and $45\text{--}123.5 \text{ m}^2/\text{g}$ when calcined, showing that the calcination increases the reactivity.
- 4) The mineralogy of LC, LN, LS and LW shows the presence of quasi-amorphous kaolinite and reactive goethite, which are responsible for the transformation of laterite to cementitious polymer structure, when attack with alkaline solution.

The particles size, the BET surface area and their significant reactivity make them promising candidates for the replacement of MK and other supplementary cementitious materials.

Declaration of competing interest

The authors declare that they have no known competing financial interests or personal relationships that could have appeared to influence the work reported in this paper.

Acknowledgments

This work was supported by Agence Universitaire de la Francophonie (AUF): Grant No 0950740/DRACGL2018 It also received the contribution of the Royal Society and the African Academy of Science through the funding FLAIR to Dr. Elie Kamseu. Grant; FLR\R1\201402. The contribution of the European Union and OEACP R&I through financial contribution No. PRICNAC-EEPER: MD2022 is greatly fully acknowledged.

Appendix A. Supplementary data

Supplementary data to this article can be found online at <https://doi.org/10.1016/j.heliyon.2023.e17750>.

References

- [1] P.K. Banerjee, *Basic Research on Laterites in Tropical Countries*, School of Oceanography, Jadavpur University, Calcutta, India, 1998.
- [2] E.A. Obonyo, E. Kamseu, P.N. Lemougna, A.B. Tchamba, U.C. Melo, C. Leonelli, A sustainable approach for the geopolymerization of natural iron-rich aluminosilicate materials, *Journal of Sustainability* (2014) 5535–5553.
- [3] E. Balan, E. Fritsch, T. Allard, G. Calas, V.S. Inheritance, Neof ormation of kaolinite during lateritic soil formation : a case study in the middle amazon basin, *Journal of Clays and clay Minerals* 55 (2007) 253–259.
- [4] M. Widdowson, in: *Book: Encyclopedia of Paleoclimatology and Ancient Environments* Edition: *Encyclopedia of Earth Sciences Series*, Springer, 2009, https://doi.org/10.1007/978-1-4020-4411-3_127. Chapter: Laterite Publisher.
- [5] E. Keskinilic, S. Pournaderi, A. Geveci, Y.A. Topkaya, Calcination Characteristics of Laterite Ores from the Central Region of Anatolia, *Journal of The Southern African Institute of Mining and Metallurgy*, 2012, p. V112 877.
- [6] A. Garces-Grand, G.T. Lapidus, O.J. Restrepo-Baena, The effect of calcination as pre treatment to enhance the nickel extraction from low-grade laterites, *Journal of Minerals Engineering* 120 (2018) 127–131.
- [7] B.P. Singh, V.K. Srivastava, Petrographical, mineralogical, and geochemical characteristics of the palaeocene lateritic bauxite deposits of kachchh basin, western India July, *Geol. J.* (2018), <https://doi.org/10.1002/gj.3313>.
- [8] G.D. Sherman, Factors Influencing the Development of Lateritic and Laterite Soils in the Hawaiian Islands, 1949, pp. 307–314.
- [9] E.J.C. Mohr, *Soils of Equatorial Regions*, 1944. Edwards Ann Arbor Michigan.
- [10] P.N. Lemougna, U.C. Melo, E. Kamseu, A.B. Tchamba, Laterite based stabilized products for sustainable building applications in tropical countries. Review and prospects for the case of Cameroon, *Journal of Sustainability* 3 (2011) 293–305.
- [11] N. Billong, U.C. Melo, F. Louvet, D. Njopwouo, Properties of compressed lateritic soil stabilized with a burnt clay-lime binder: effect of mixture components, *Journal of Construction and Building Materials* 23 (2009) 2457–2460.
- [12] C.R. Kaze, P. Venyite, A. Nana, N.J. Deutou, H.K. Tchakoute, H. Rahier, E. Kamseu, C.U. Melo, L. Cristina, Meta-halloysite to improve compactness in iron-rich laterite-based alkali activated materials, *Journal of Materials Chemistry and Physics* 19 (2020), <https://doi.org/10.1016/j.matchemphys.2019.122268>.
- [13] H.A. Abdel-Gawwad, K.A. Metwally, T.A. Tawfik, M.S. Mohammed, S.H. Hassan, M. Heikal, I.M. El- Kattan, Evaluating the performance of high volume fly ash-blended-cement mortar individually containing nano- and ultrafine micro-magnesia, *J. Build. Eng.* 36 (2021), <https://doi.org/10.1016/j.job.2020.102129>.
- [14] A.T. Bakera, G.A. Mark, Use of metakaolin as a supplementary cementitious material in concrete , with a focus on durability properties, *RILEM Technical Letters* 4 (2019) 89–102.
- [15] E. Badogiannis, G. Kakali, S. Tsvilivis, Metakaolin as supplementary cementitious material : optimization of kaolin to metakaolin conversion, *J. Therm. Anal. Calorim.* 81 (2005) 457–462, <https://doi.org/10.2298/HEMIND100322014I>.
- [16] A. Albidah, M. Alghannam, H. Abbas, T. Almusallam, Y. Al-Salloum, Characteristics of metakaolin-based geopolymer concrete for different mix design parameters, *J. Mater. Res. Technol.* 10 (2021) 84–98.
- [17] F.K. Alqahatani, K. Rashid, I. Zafar, M.I. Khan, A.A. Ababtain, Production of sustainable green mortar by ultrahigh utilization of fly ash. Technical, economic and environmental assessment, *Journal of Construction and Building Materials* 281 (2021), 122617.
- [18] Y. Wang, P. Suraneni, Experimental methods to determine the feasibility of steel slags as supplementary cementitious materials, *Journal of Construction and Building Materials* 204 (2019) 458–467.
- [19] M.C.G. Juenger, R. Snellings, S.A. Bernal, Supplementary cementitious materials: new sources, characterization, and performance insights, *Cement Concr. Res.* 122 (2019) 257–273.
- [20] J.N. Nouping Fekoua, C.R. Kaze, L. Duna, A. Ghazouni, I.M. Ndassa, E. Kamseu, S. Rossignol, C. Leonelli, Effects of curing cycles on developing strength and microstructure of goethite-rich aluminosilicate (corroded laterite) based geopolymer composites, *Journal of Materials Chemistry and Physics* 270 (2021), <https://doi.org/10.1016/j.matchemphys.2021.124864>.
- [21] R.Y. Nkwajui, J.N.Y. Djobo, J.N.F. Nouping, P.W.M. Huisken, J.G.N. Deutou, L. Courard, Iron-rich laterite-bagasse fibers based geopolymer composite: mechanical, durability and insulating properties, *Journal of Applied Clay Science* 183 (2019), <https://doi.org/10.1016/j.clay.2019.105333>.
- [22] A.B. Tchamba, R. Yongue, U.C. Melo, E. Kamseu, D. Njoya, *DJOPWOUO Caractérisation de la bauxite de Haléo - danielle (Minim - martap, Cameroun) en vue de son utilisation industrielle dans les matériaux à haute teneur en alumine*, *Journal of silicate industriel* 73 (2008) 5–6.
- [23] A.L. Velosa, F. Rocha, R. Veiga, Influence of chemical and mineralogical composition of metakaolin on mortar characteristics, *Acta Geodyn. Geomater.* 6 (2009) 121–126.
- [24] S.C. Devi, R.A. Khan, B.S. Rautela, Influence of metakaolin on chemical resistance of low calcium fly ash based geopolymer, *Journal of Concrete. Materials Science and Engineering* 431 (2018), <https://doi.org/10.1088/1757-899X/431/9/092008>.
- [25] A. Haris Subaer, A. Irahmsyah, A.D. Permatasari, Pervaporation membrane based on laterite zeolite-geopolymer for Ethanol/Water separation, *J. Clean. Prod.* 19 (2019), <https://doi.org/10.1016/j.jclepro.2019.119413>.
- [26] F.J.N. Nouping, C.R. Kaze, L.D. Linda, A. Ghazouni, I.N. Mboumbouo, E. Kamseu, S. Rossignol, C. Leonelli, Effects of curing cycles on developing strength and microstructure of goethite-rich aluminosilicate (corroded laterite) based geopolymer composites, *Journal of Materials Chemistry and Physics* 270 (2021), <https://doi.org/10.1016/j.matchemphys.2021.124864>.
- [27] A.K. Panda, B.G. Mishra, D.K. Mishra, R.K. Singh, *Colloids and surfaces A : physicochemical and engineering aspects effect of sulphuric acid treatment on the physico-chemical characteristics of kaolin clay*, *Journal of Colloids and Surfaces A: Physicochemical and Engineering Aspects* 363 (2010) 98–104.

- [28] P. Venyite, E.C. Makone, R.C. Kaze, A. Nana, J.G.N. Deutou, E. Kamseu, U.C. Melo, C. Leonelli, Effect of Combined Metakaolin and Basalt Powder Additions to Laterite-Based Geopolymers Activated by Rice Husk Ash (RHA) /NaOH Solution, Check for Updates, 2021, <https://doi.org/10.1007/s12633-021-00950-7>.
- [29] P. Ptacek, F. Frajkorova, F. Soukal, T. Opravil, Kinetics and mechanism of three stages of thermal transformation of kaolinite to metakaolinit, Journal of Powder Technology 264 (2014) 439–445, <https://doi.org/10.1016/j.powtec.2014.05.04>.
- [30] R.I. Biljana, M. Aleksandra, M. Ljiljana, Thermal Treatment of kaolin clay to obtain metakaolin, Hem. Ind. 64 (2010) 351–356.
- [31] C. Li Wang, Z. Peng, S. Zhang, Characterization and Thermal Behavior of Kaolin Journal of Thermal Analysis and Calorimetry 105 (2011) 157–160.
- [32] R.P. Dos Santos, J. Martins, C. Gadelha, B. Cavada, A.V. Albertini, F. Arruda, M. Vasconcelos, E. Teixeira, F. Alves, J.L. Filho, V. Freire, Coal fly ash ceramics: preparation, characterization, and use in the hydrolysis of sucrose, Sci. World J. (2014) 1–7.
- [33] A. Kielé, D. Vaičiukynienė, G. Tamošaitis, R. Bistrickaitė, Thermal properties of alkali activated slag plaster for wooden structures, Sci. Rep. (2020), <https://doi.org/10.1038/s41598-020-57515-8>.
- [34] E. Kamseu, V. Alzari, D. Nuvoli, D. Sanna, I. Lancellotti, A. Mariani, C. Leonelli, Dependence of the geopolymerization process and end-products to the nature of solid precursors: challenge of the sustainability, J. Clean. Prod. 278 (2021), <https://doi.org/10.1016/j.jclepro.2020.123587>.
- [35] C. Panagiotopoulou, E. Kontori, T. Perraki, G. Kakali, Dissolution of aluminosilicate minerals and by-products in alkaline media, J. Mater. Sci. 42 (2007) 2967–2973.
- [36] E. Kamseu, C.R. Kaze, J.N. Nouping Fekoua, U.C. Melo, S. Rossignol, C. Leonelli, Ferrisilicates formation during the geopolymerization of natural Fe-rich aluminosilicate precursors, journal of Materials Chemistry and Physics 240 (2020).